Talanta 85 (2011) 2620–2625

Contents lists available at ScienceDirect

Talanta

journal homepage: www.elsevier.com/locate/talanta

A novel lable-free electrochemical immunosensor for carcinoembryonic antigen based on gold nanoparticles–thionine–reduced graphene oxide nanocomposite film modified glassy carbon electrode

Fen-Ying Kong[a,b], Mao-Tian Xu[b], Jing-Juan Xu[a,*], Hong-Yuan Chen[a]

[a] State Key Lab of Analytical Chemistry for Life Science, School of Chemistry and Chemical Engineering, Nanjing University, Nanjing 210093, People's Republic of China
[b] Department of Chemistry, Shangqiu Normal University, Shangqiu 476000, People's Republic of China

ARTICLE INFO

Article history:
Received 25 May 2011
Received in revised form 10 August 2011
Accepted 13 August 2011
Available online 19 August 2011

Keywords:
Label-free
Gold nanoparticles
Reduced graphene oxide
Thionine
Carcinoembryonic antigen

ABSTRACT

In this paper, gold nanoparticle–thionine–reduced graphene oxide (GNP–THi–GR) nanocomposites were prepared to design a label-free immunosensor for the sensitive detection of carcinoembryonic antigen (CEA). The nanocomposites with good biocompatibility, excellent redox electrochemical activity and large surface area were coated onto the glassy carbon electrode (GCE) surface and then CEA antibody (anti-CEA) was immobilized on the electrode to construct the immunosensor. The morphologies and electrochemistry of the formed nanocomposites were investigated by using scanning electron microscopy (SEM), ultraviolet–visible (UV–vis) spectrometry, electrochemical impedance spectroscopy (EIS) and cyclic voltammetry (CV). CV and differential pulse voltammetry (DPV) studies demonstrated that the formation of antibody–antigen complexes decreased the peak current of THi in the GNP–THi–GR nanocomposites. The decreased currents were proportional to the CEA concentration in the range of 10–500 pg/mL with a detection limit of 4 pg/mL. The proposed method was simple, fast and inexpensive for the determination of CEA at very low levels.

1. Introduction

Carcinoembryonic antigen (CEA), is one of the most extensively used clinical tumor marker. It was first described in 1965 as a marker of colon cancer, and was expressed in many malignancies, such as lung cancer [1,2], ovarian carcinoma [3], breast cancer [4–6], and cystadenocarcinoma [7]. Therefore, sensitive determination of CEA is very important in clinical research and diagnosis.

Graphene has recently attracted much attention for its unique electronic properties, large specific surface area, potentially low manufacturing cost, excellent mechanical properties, and superior thermal properties [8–14]. Owing to all of these exceptional properties, graphene finds potential application in microelectronics [15–17], large-area optoelectronics [18–20], sensors [21–23], actuators [24] and so forth. Among them, of particular interest for us is to explore its application in the field of electrochemical sensor. The high surface area is helpful in increasing the surface loading of the target molecules. The excellent conductivity and small band gap are favorable for conducting electrons from biomolecules [13]. Graphene-based materials have been reported one after the other to fabricate electrochemical sensors, such as electrochemical determination of glucose [25,26], β-NADH [27], dopamine [28] and cytochrome *c* [29]. More recently, Lin et al. explored the graphene-based immunosensor [30]. Gong and co-workers used graphene-based nanomaterials for the ultrasensitive detection of cancer biomarker [31]. Zhang's group used nanogold-enwrapped graphene nanocomposites as tracer labels to quantify carcinoembryonic antigen [32]. These results indicated that graphene-based materials possessed a great potential to fabricate the electrochemical sensor.

In this paper, we proposed a new lable-free electrochemical immunosensor based on the graphene material. First we prepared the gold nanoparticle–thionine–reduced graphene oxide (GNP–THi–GR) nanocomposites. To fabricate the nanocomposites, THi was initially noncovalently bound to the GR sheet through π–π stacking to form a novel redox active hybrid material (THi–GR). Subsequently, GNPs were anchored to the surface of THi–GR by the chemisorption of the amine groups of the THi and the opposite-charged adsorption. Herein, THi not only acts as an electrochemical active species but also acts as a "glue" to connect the GNPs to the GR sheets. As shown in Fig. 1. The resulting GNP–THi–GR nanocomposites combined the following advantages: (1) GR possesses fast electron transfer kinetics and large specific surface area; (2) THi has good electrochemical redox active properties; (3) GNPs can provide a microenvironment to retain the proteins conformation and make them free in orientation [33]. In addition, the GNPs could

* Corresponding author. Tel.: +86 25 83597294; fax: +86 25 83597294.
E-mail address: xujj@nju.edu.cn (J.-J. Xu).

0039-9140/$ – see front matter © 2011 Elsevier B.V. All rights reserved.
doi:10.1016/j.talanta.2011.08.028

effectively promote electronic transfer [34]. So, the immunosensors based on the GNP–THi–GR nanocomposites significantly enhanced the sensitivity and greatly simplified the assay system.

2. Experimental

2.1. Reagents

Graphite powder, trisodium citrate and thionine acetate salt were obtained from Shanghai Biochemical Reagent Company (Shanghai, China). Chloroauric acid ($HAuCl_4$), lyophilized bovine serum albumin (BSA), CEA and CEA antibody (anti-CEA) were purchased from Sigma (St. Louis, USA). GNPs with mean size of 16 nm were prepared by citrate reduction of $HAuCl_4$ in aqueous solution at 100 °C for half an hour [35]. Phosphate buffer solution (PBS, 0.1 mol/L, pH 6.0) was used as working solution. All solvents were of analytical grade. Ultrapure water from a Milli-Q plus system (Millipore Co., >18 MΩ cm) was used in all aqueous solutions and rinsing procedures. The healthy people's serum specimens supplied by Central Hospital of Shangqiu were diluted to different concentrations with PBS of pH 6.0.

2.2. Apparatus

Electrochemical measurements were recorded using a CHI 660D electrochemical workstation (Shanghai, China) with a conventional three electrode system comprised of platinum wire as the auxiliary electrode, saturated calomel electrode (SCE) as the reference electrode and modified glassy carbon electrode (GCE, 3 mm in diameter) as the working electrode. The electrochemical impedance spectroscopy (EIS) measurements were performed in the solution of 0.10 mol/L KCl containing 5.0 mmol/L $K_3[Fe(CN)_6]/K_4[Fe(CN)_6]$ (1:1) mixture as a redox probe at a bias potential of 0.20 V. The alternative voltage was 5 mV and the frequency range was $0.1–1.0 \times 10^5$ Hz. The ultraviolet–visible (UV–vis) spectrometry was acquired with a UV 2300 spectrophotometer (Shanghai, China). Scanning electron microscopy (SEM) images were obtained using an S-3000 N scanning electron microscope (Tokyo, Japan). Ultrasonication was performed using a KQ-100E ultrasonic cleaner (Kunshan, China). All experiments were performed at room temperature.

2.3. Preparation of GR

Graphene oxide (GO) was first synthesized from natural graphite powder using a modified Hummers and Offeman's method [36]. GR was prepared by the chemical reduction of GO according to the literature with a little modification [37]. Briefly, the resulting GO dispersion (100 mL) was mixed with certain amount of ascorbic acid solution. Then the mixture was treated by ultrasonication for 1 h at 60 °C. The obtained black suspension was washed with water for several times and dried in vacuum at 60 °C overnight.

2.4. Preparation of GNP–THi–GR nanocomposites

In a typical procedure, the as-prepared GR (1 mg) were dispersed in 1 mL water by ultrasonication, and then mixed with 1 mL of 1 mmol/L THi solution at room temperature for at least 12 h. After discarding the supernatant, the THi–GR nanocomposites again were dispersed in 1 mL water. Subsequently, the THi–GR nanocomposites were added dropwise into 20 mL of the as-prepared GNPs. The mixture was allowed to react at room temperature under stirring for 24 h, followed by centrifugation. The resulting GNP–THi–GR nanocomposites were washed with water and then re-dispersed in 1 mL of PBS (pH 7.4) buffer and stored at 4 °C before use.

2.5. Fabrication of the immunosensor

Glassy carbon electrode (GCE) was polished down to mirror-like with 1.0 and 0.3 μm alumina slurry, followed by successive ultrasonication in distilled water and ethanol for 5 min and dried in air. Afterwards, 5 μL GNP–THi–GR nanocomposites were dipped onto the surface of the GCE, and dried for 2 h at room temperature. The obtained electrode was immersed in the anti-CEA solution and incubated for more than 12 h at 4 °C. Then, unbound antibodies were washed away with PBS. Subsequently, the as-prepared immunosensor was incubated in 1% BSA for 1 h at 37 °C to block possible remaining active sites and avoid the nonspecific adsorption. After washed carefully for three times with PBS, the electrode was stored at 4 °C while not in use. The fabrication process of the electrochemical immunosensor is schematically illustrated in Fig. 1.

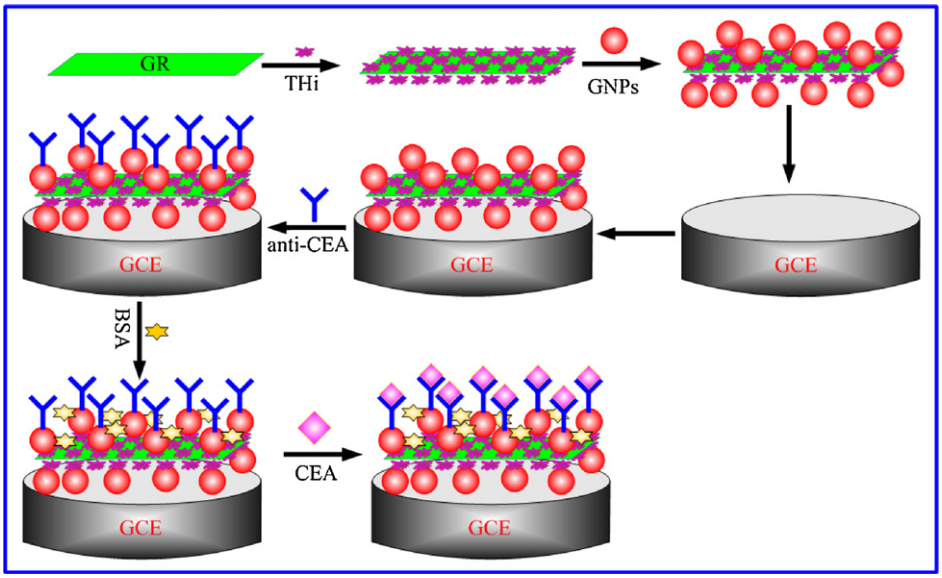

Fig. 1. Preparation process of the GNP–THi–GR nanocomposites and immunosensor.

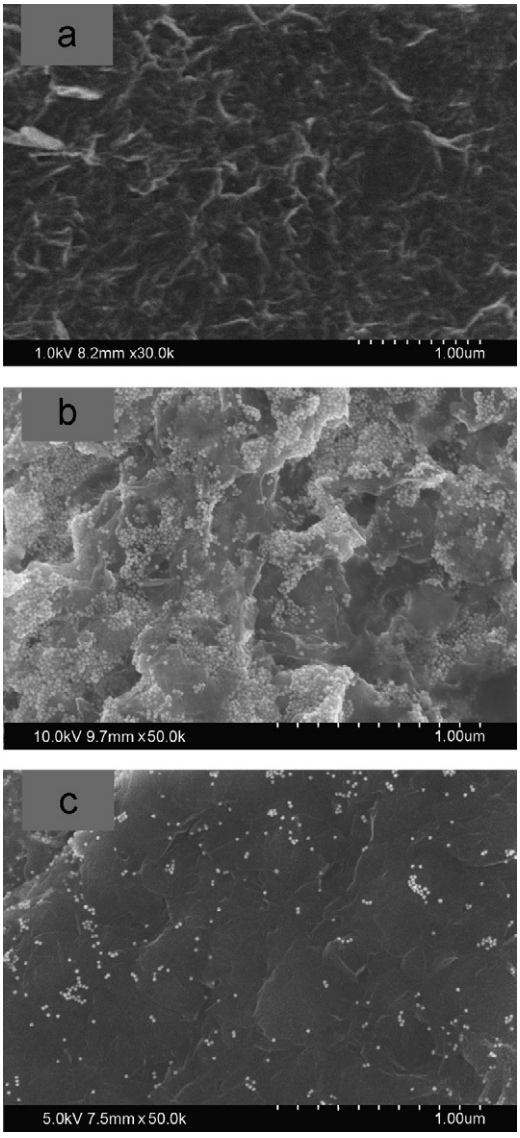

Fig. 2. SEM images of GR (a), GNP–THi–GR nanocomposites (b) and GNP–GR nanocomposites (c).

2.6. Electrochemical measurement procedures

The prepared immunosensor was incubated in 100 μL incubation solution containing different concentration of CEA at 37 °C for 10 min. After the residual was removed with PBS, differential pulse voltammetry (DPV) from 0.2 to −0.6 V (vs. SCE) was recorded in 0.1 mol/L PBS (pH 6.0). The measurement principle was based on the inhibition of the response current of THi in the GNP–THi–GR nanocomposites after the formation of antigen–antibody complex, which was directly proportional to the concentration of CEA.

3. Results and discussion

3.1. Characterization of the GNP–THi–GR nanocomposites

The morphology of GR, GNP–GR and GNP–THi–GR nanocomposites were characterized by SEM technique. The SEM image of GR (Fig. 2a) showed a wrinkled paper-like structure with irregular size. These wrinkles are important for preventing the aggregation of graphene during drying and maintaining a high surface area [38,39]. From Fig. 2b, it can be clearly seen that GNPs were

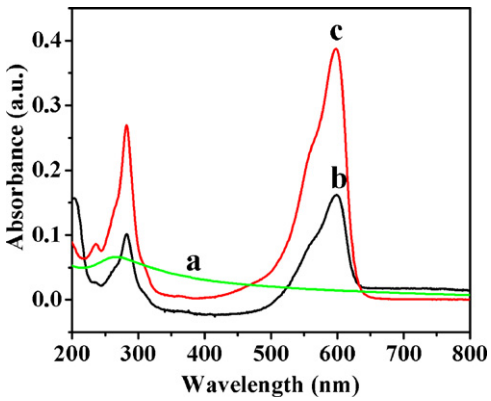

Fig. 3. UV–vis absorption spectra of GR (a), THi–GR (b) and pure THi solution (c).

bound on THi–GR surface with dense distribution, indicating the strong interaction between the GNPs and the THi–GR nanocomposite. For comparison, we mixed the GR with the GNPs without THi molecules, and observed few GNPs anchored on the GR sheets (Fig. 2c), indicating the important role of THi molecules play in the binding of GNPs to the GR sheet.

UV–vis spectrometry was employed to explore the interactions between GR and THi. Fig. 3 showed the typical UV–vis spectra of GR (a), THi–GR (b) and pure THi solution (c). The spectrum of GR showed an absorption band at about 266 nm (curve a), which corresponded to the chemically reduced GO [40]. Two absorption bands at 280 and 599 nm were observed at THi–GR nanocomposite (curve b). In comparison with those obtained at pure THi solution (curve c), the slightly red shift and broadened for the absorption band at 599 nm provided further evidence for the formation of THi–GR nanocomposite. This phenomenon was consistent with the reported literature [31].

3.2. Electrochemical characteristics of the immunosensor

In order to confirm that the sensing interface has been constructed successfully, we utilized EIS to monitor the impedance change of each modification process. The results were shown in Fig. 4. It was observed that the bare GCE showed a small well semicircle domain at higher frequencies (curve a). After the electrode was modified with GNP–THi–GR nanocomposites, the semicircle domain became smaller in curve b. The reason may be that THi as an excellent electron transfer mediator and GR together with GNPs in the GNP–THi–GR nanocomposites possessing good

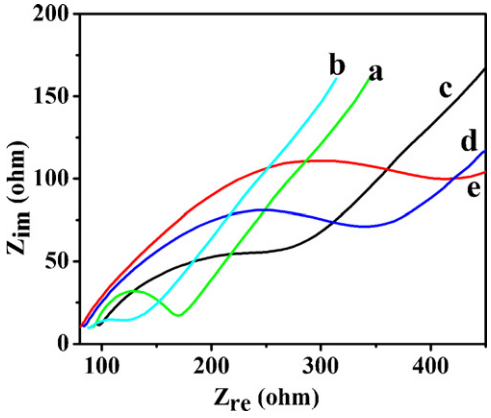

Fig. 4. EIS of bare GCE (a), GNP–THi–GR/GCE (b), anti-CEA/GNP–THi–GR/GCE (c), BSA/anti-CEA/GNP–THi–GR/GCE (d) and CEA/BSA/anti-CEA/GNP–THi–GR/GCE (e) in 5 mmol/L $K_3Fe(CN)_6/K_4Fe(CN)_6$ (1:1) solution containing 0.1 mol/L KCl.

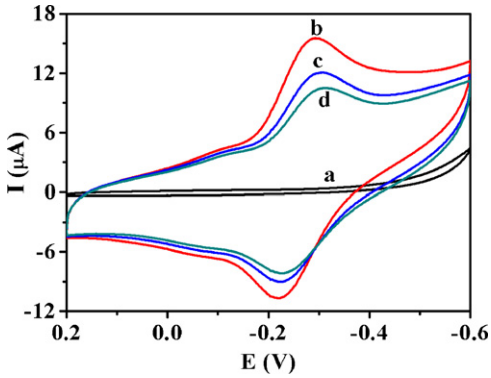

Fig. 5. The different modified electrodes in 0.1 mol/L PBS: (a) bare GCE, (b) GNP–THi–GR/GCE, (c) anti-CEA/GNP–THi–GR/GCE, and (d) BSA/anti-CEA/GNP–THi–GR/GCE, all potentials were given vs. SCE and the scan rate was 50 mV/s.

conductive properties are favorable for the electron transfer. After the GNP–THi–GR/GCE was incubated with anti-CEA, a large semicircle domain was found in curve c. Subsequently, when BSA was adsorbed on the surface, the electron-transfer resistance obviously increased (curve d). At last, after CEA was coupled onto the BSA/anti-CEA/GNP–THi–GR/GCE, an increase of interfacial resistance was obtained (curve e). The reason may be that the outer protein membrane on the electrode acts as the electron communication and mass-transfer blocking layer, further insulating the conductive support and counteracting the interfacial electron transfer [41].

On the other hand, cyclic voltammetry (CV) was employed to monitor each immobilization step and the corresponding results were shown in Fig. 5. It can be seen that the bare GCE had no redox peak in PBS solution (curve a) for the absence of redox probes. Then a pair of well-defined redox peak was appeared in curve b with GNP–THi–GR nanocomposites modified GCE. Therefore, these two peaks were from the redox reaction of THi in the GNP–THi–GR nanocomposites. However, the loading of anti-CEA led to a decrease of the redox peak currents (curve c). After the modified electrode was immersed in BSA, a further decrease of the current can be observed (curve d). These measurements were in good agreement with the results obtained from EIS.

Moreover, The CVs of the resulting immunosensor in PBS (pH 6.0) at different scan rates were also studied. The results were shown in Fig. 6. It can be observed that the couple of redox peak currents increased with the increase of potential scan rate. In addition, both the anodic and cathodic peak currents were directly

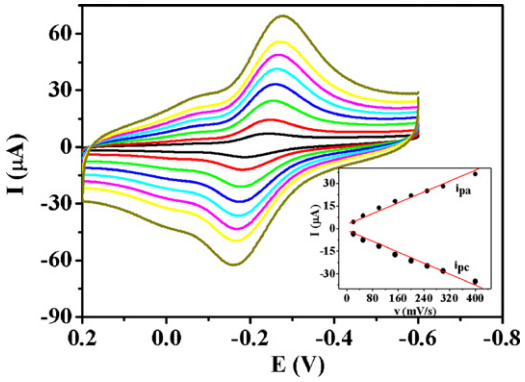

Fig. 6. Cyclic voltammograms of the modified electrode at different scan rates (from inner to outer): 20, 50, 100, 150, 200, 250, 300 and 400 mV/s in 5 mL 0.1 mol/L PBS (pH 6.0) under room temperature. The inset shows the dependence of redox peak currents on the potential sweep rates.

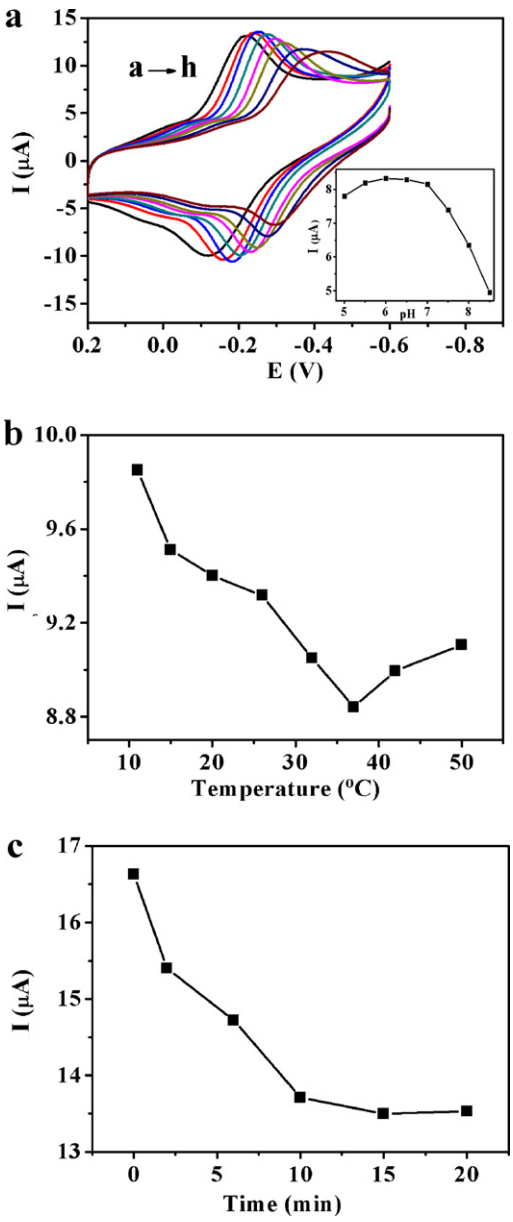

Fig. 7. Effects of (a) pH of detection solution, (b) incubation temperature, and (c) incubation time on the immunosensor.

proportional to the potential scan rates in the range of 20–400 mV/s (shown in the inset), suggesting a surface confined redox process [42].

3.3. Optimization of analytical conditions for immunoassay

The pH of the supporting electrolyte would influence the electrochemical response of the immunosensor. Unsuitable pH may cause protein denaturalization. In addition, the pH may affect the electrochemical behavior of the THi. In order to optimize the pH, a series of PBS solutions with the pH from 5.0 to 8.5 were prepared and the immunosensors were tested by CVs (Fig. 7a, a–h, scan rate 50 mV/s). It was found that the immunosensor exhibited a maximal current response at pH 6.0 PBS and an increase in pH led to a decrease of the redox peak current (Fig. 7a, inset). The reason was that the reduction and the oxidation of THi need the participation of proton. Thus, the optimal pH of 6.0 was chosen in the further study.

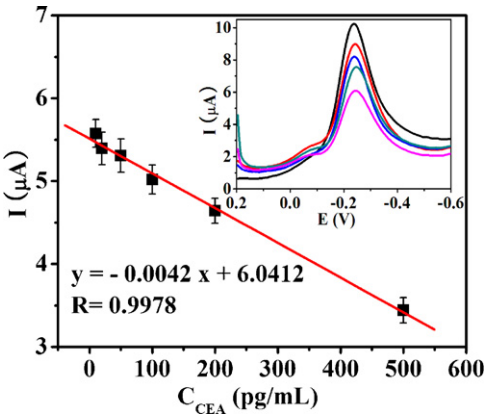

Fig. 8. The calibration curve of the immunosensor for CEA determination. Inset: DPV curves of the immunosensor after incubating with different CEA solutions with concentrations of 0, 10, 50, 200, and 500 pg/mL (from top to bottom).

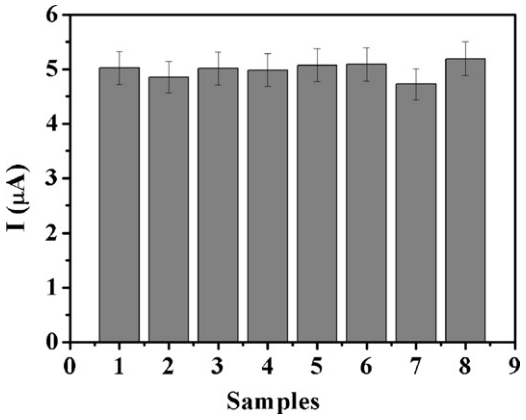

Fig. 9. Current response of the immunosensor to 100 pg/mL CEA (1), (1) +1 ng/mL IgG (2), (1) +1 ng/mL BSA (3), (1) +1 ng/mL AA (4), (1) +1 ng/mL lysine (5), (1) +1 ng/mL cysteine (6), (1) +1 ng/mL glutamate (7), (1) +1 ng/mL glucose (8). Error bar = RSD (n = 5).

To acquire a high electrochemical response, incubated conditions such as incubation temperature and incubation time for the antigen–antibody reaction should be optimized. The effect of incubation temperature on the immunosensor was studied in the range from 20 to 42 °C as shown in Fig. 7b. The current response decreased with increasing temperature up to 37 °C, while the temperature over 37 °C, the current response began to increase, implying a favor of the physiological temperature about the immunoreaction. Thus, the incubation temperature was chosen to be 37 °C. At this temperature, we investigated the effect of the incubation time on the current response (Fig. 7c, scan rate 100 mV/s). It was found that the response signal decreased with the incubation time up to 10 min and then tended to level off, which indicated an equilibration state was reached. Therefore, 10 min of incubation time was used for the detection of CEA.

3.4. Performance of the immunosensor

Under the optimal conditions, the DPV response of the immunosensor to CEA was investigated. As expected, the current response signal decreased with increase of CEA concentration because antigen–antibody complex acting as an inert block layer hindered the electron transfer toward the electrode surface. The calibration plots were obtained by recording the current response versus the different concentrations of CEA standard solutions (Fig. 8). The linear range spans the concentration of CEA from 10 to 500 pg/mL, with a correlation coefficient of 0.9978. The linear regression equation was $y = -0.0042x + 6.0412$ and a detection limit was estimated at 4 pg/mL (S/N = 3). The performances of the developed CEA immunosensors were superior to those of other immunosensors reported in the literatures [43–48], especially the detection limit.

3.5. Selectivity, reproducibility and stability of immunosensors

Selectivity is a crucial parameter which influences the performance. Thus, the potential interferents, including human IgG, BSA, vitamin C, L-lysine, L-cysteine, L-glutamate and glucose were studied. The 100 pg/mL of CEA solution containing 1 ng/mL of interfering substances was tested by the immunosensor and the results are shown in Fig. 9. The current variation due to the interfering substances was less than 6% of that without interferences, indicating the selectivity of the immunosensor was satisfactory.

To evaluate the reproducibility of the immunosensors, a series of five electrodes were prepared for detecting 100 pg/mL CEA. The relative standard deviation (RSD) of the measurements for the five electrodes was 4.6%, suggesting the precision and reproducibility of the immunosensor was quite good. The stability of the successive assays was studied. After 50 CV measurements in PBS, a RSD of 3.2% was acquired. The long-time stability of the immunosensor was also investigated. When not in use, the electrode was stored in PBS at 4 °C. After two weeks, the response of the immunosensor retained about 90% of its initial value. The good stability may be due to the fact that the protein molecules were attached firmly onto the surface of GNP–THi–GR nanocomposites.

Table 1
Recovery of prepared immunosensor.

Sample	Standard value of CEA (pg/mL)	Found (pg/mL)	Recovery (%)
1	40	45.20	113
2	80	78.98	98.7
3	100	92.46	92.5
4	150	142.87	95.3
5	200	207.94	104

3.6. Real sample analysis

To examine the applicability and reliability of using the present immunosensor for practical analyses, recovery experiments were performed by standard addition methods in human serum. Several freeze-drying standard samples were dissolved in the human serum samples with concentrations from 40 pg/mL to 200 pg/mL and analyzed by using the proposed immunosensor. The experimental results are listed in Table 1. It showed an acceptable recovery in the range of 92.5–113%. This result also indicated that the present immunosensor might provide a feasible alternative tool for determining CEA in human serum for routine clinical diagnosis.

4. Conclusions

In this paper, we had synthesized GNP–THi–GR nanocomposites using THi molecules as interlinkers. The π–π stacking interactions between GR and THi, and the interaction between the amine groups in THi and GNPs together with the electrostatic interaction between THi and GNPs, resulted in the formation of GNP–THi–GR nanocomposites. Based on this nanocomposite film, a sensitive and label-free immunosensor for CEA determination was developed. It was worth noting that the as-prepared nanocomposites in our work combined the advantages of the GR (unique electrical conductivity, enlarged active surface area) and THi (excellent redox activity) together with GNPs (excellent biocompatibility). Therefore, the immunosensor

exhibited a highly response sensitivity, a low detection limit, good stability and a wide linear range to CEA.

Acknowledgments

This work was supported by the NSFC (Grant nos. 21025522, 20890021), the NSFC for Creative Research Groups (Grant no. 20821063).

References

[1] L. Hernandez, A. Espasa, C. Fernandez, A. Candela, C. Martin, S. Romero, Lung Cancer 36 (2002) 83.
[2] T. Iwazawa, T. Kanoh, S. Matsui, Lung Cancer 29 (2000) 254.
[3] D.A. Gould, G.J. Moscoso, M.P.A. Young, J. Soc. Gynecol. Investig. 7 (2000) 131.
[4] S. Kramer, W. Jager, N. Lang, Eur. J. Cancer A 34 (1998) s42.
[5] C. Cameiro, L. Costa, M. Melo, Eur. J. Cancer A 34 (1998) s43.
[6] B. Sahin, V. Paydak, S. Paydas, Eur. J. Cancer 32 (1996) s24.
[7] K. Kazuya, K. Yoshihiro, K. Tsunekazu, Gynecol. Obstet. Invest. 47 (1999) 52.
[8] D.W. Wang, F. Li, Z.S. Wu, W. Ren, H.M. Cheng, Electrochem. Commun. 11 (2009) 1729.
[9] S. Stankovich, D.A. Dikin, R.D. Piner, K.A. Kohlhaas, A. Kleinhammes, Y. Jia, Y. Wu, S.T. Nguyen, R.S. Ruoff, Carbon 45 (2007) 1558.
[10] X.L. Li, G.Y. Zhang, X.D. Bai, X.M. Sun, X.R. Wang, E. Wang, H.J. Dai, Nat. Nanotechnol. 3 (2008) 538.
[11] S. Park, R.S. Ruoff, Nat. Nanotechnol. 4 (2009) 217.
[12] K.S. Novoselov, A.K. Geim, S.V. Morozov, D. Jiang, Y. Zhang, S.V. Dubonos, I.V. Grigorieva, A.A. Firsov, Science 306 (2004) 666.
[13] S. Stankovich, D.A. Dikin, G.H.B. Dommett, K.M. Kohlhaas, E.J. Zimney, E.A. Stach, R.D. Piner, S.T. Nguyen, R.S. Ruoff, Nature 442 (2006) 282.
[14] C. Lee, X. Wei, J.W. Kysar, J. Hone, Science 321 (2008) 385.
[15] K.S. Novoselov, A.K. Geim, S.V. Morozov, D. Jiang, M.I. Katsnelson, I.V. Grigorieva, S.V. Dubonos, A.A. Firsov, Nature 438 (2005) 197.
[16] S.V. Morozov, K.S. Novoselov, M.I. Katsnelson, F. Schedin, D.C. Elias, J.A. Jaszczak, A.K. Geim, Phys. Rev. Lett. 100 (2008) 016602.
[17] B. Li, X. Cao, H.G. Ong, J.W. Cheah, X. Zhou, Z. Yin, H. Li, J. Wang, F. Boey, W. Huang, H. Zhang, Adv. Mater. 22 (2010) 3058.
[18] Q.L. Bao, H. Zhang, Y. Wang, Z.H. Ni, Y.L. Yan, Z.X. Shen, K.P. Loh, D.Y. Tang, Adv. Funct. Mater. 19 (2009) 3077.
[19] X. Wang, L. Zhi, K. Mullen, Nano Lett. 8 (2008) 323.
[20] Z. Yin, S. Wu, X. Zhou, X. Huang, Q. Zhang, F. Boey, H. Zhang, Small 6 (2010) 307.
[21] F. Schedin, A.K. Geim, S.V. Morozov, E.W. Hill, P. Blake, M.I. Katsnelson, K.S. Novoselov, Nat. Mater. 6 (2007) 652.
[22] Q. He, H.G. Sudibya, Z. Yin, S. Wu, H. Li, F. Boey, W. Huang, P. Chen, H. Zhang, ACS Nano. 4 (2010) 3201.
[23] Z. Wang, X. Zhou, J. Zhang, F. Boey, H. Zhang, J. Phys. Chem. C 113 (2009) 14071.
[24] J.S. Bunch, S.S. Verbridge, J.S. Alden, A.M. van der Zande, J.M. Parpia, H.G. Craighead, P. McEuen, Nano Lett. 8 (2008) 2458.
[25] C.S. Shan, H.F. Yang, J.F. Song, D.X. Han, A. Ivaska, L. Niu, Anal. Chem. 81 (2009) 2378.
[26] T.T. Baby, S.S. Jyothirmayee Aravind, T. Arockiadoss, R.B. Rakhi, S. Ramaprabhu, Sens. Actuators B 145 (2010) 71.
[27] W.J. Lin, C.S. Liao, J.H. Jhang, Y.C. Tsai, Electrochem. Commun. 11 (2009) 2153.
[28] Y. Wang, Y. Li, L. Tang, J. Lu, J. Li, Electrochem. Commun. 11 (2009) 889.
[29] J.F. Wu, M.Q. Xu, G.C. Zhao, Electrochem. Commun. 12 (2010) 175.
[30] D. Du, Z.X. Zou, Y. Shin, J. Wang, H. Wu, M.H. Engelhard, J. Liu, I.A. Aksay, Y.H. Lin, Anal. Chem. 82 (2010) 2989.
[31] M.H. Yang, A. Javadi, H. Li, S.Q. Gong, Biosens. Bioelectron. 26 (2010) 560.
[32] Z.Y. Zhong, W. Wu, D. Wang, D. Wang, J.L. Shan, Y. Qing, Z.M. Zhang, Biosens. Bioelectron. 25 (2010) 2379.
[33] C.R. Martin, D.T. Mitchell, Anal. Chem. 70 (1998) 322.
[34] K.J. Feng, C.H. Sun, Y. Kang, J.W. Chen, J.H. Jiang, G.L. Shen, R.Q. Yu, Electrochem. Commun. 10 (2008) 531.
[35] B.V. Enüstün, J. Turkevich, J. Am. Chem. Soc. 85 (1963) 3317.
[36] W.S. Hummers, R.E. Offeman, J. Am. Chem. Soc. 80 (1958) 1339.
[37] J. Gao, F. Liu, Y.L. Liu, N. Ma, Z.Q. Wang, X. Zhang, Chem. Mater. 22 (2010) 2213.
[38] H.C. Schniepp, J.L. Li, M.J. McAllister, H. Sai, M.H. Alonso, D.H. Adamson, R.K. Prud'homme, R. Car, D.A. Saville, I.A. Aksay, J. Phys. Chem. B 110 (2006) 8535.
[39] M.J. McAllister, J.L. Li, D.H. Adamson, H.C. Schniepp, A.A. Abdala, J. Liu, M. Herrera-Alonso, D.L. Milius, R. Car, I.A. Aksay, Chem. Mater. 19 (2007) 4396.
[40] H. Liu, J. Gao, M.Q. Xue, N. Zhu, M.N. Zhang, T.B. Cao, Langmuir 25 (2009) 12006.
[41] Y. Zhuo, R. Yuan, Y.Q. Chai, D.P. Tang, Y. Zhang, N. Wang, X.L. Li, Q. Zhu, Electrochem. Commun. 7 (2005) 355.
[42] H.C. Yoon, M.Y. Hong, H.S. Kim, Anal. Chem. 72 (2000) 4420.
[43] D.Y. Tang, B.Y. Xia, Microchim. Acta 163 (2008) 41.
[44] X.T. Zhang, Y.F. Wu, Y.F. Tu, S.Q. Liu, Analyst 133 (2008) 485.
[45] Y. Zhuo, R.J. Yu, R. Yuan, Y.Q. Chai, C.L. Hong, J. Electroanal. Chem. 628 (2009) 90.
[46] K. Huang, D. Niu, W. Xie, W. Wang, Anal. Chim. Acta 659 (2010) 102.
[47] J. Wu, F. Yan, X. Zhang, Y. Yan, J. Tang, H. Ju, Clin. Chem. 54 (2008) 1481.
[48] H.F. Chen, J. Tang, B.L. Su, G.N. Chen, J.X. Huang, D.P. Tang, Anal. Chim. Acta 678 (2010) 169.